

**GT2011-46854**

**Flow Distribution and Heat Transfer Coefficients inside Gas Holes Discharging into an Orthogonal Crossflow**

**S. Acharya and A. Eshtiaghi**

Turbine Innovation and Energy Research (TIER) Center  
 Louisiana State University  
 Baton Rouge, LA, USA

**R. Schilp**

Gas Turbine Engineering  
 Siemens Energy  
 Orlando, FL, USA

**ABSTRACT**

Fluid flow and heat transfer coefficient associated with flow inside short holes ( $L/D=1$ ) discharging orthogonally into a crossflow was investigated experimentally and numerically for  $\overline{Re}$  ranging from  $0.5 \times 10^5$  to  $2 \times 10^5$ , and blowing ratio ranging from 1.3 to 3.2. The basic configuration studied consists of a feed tube with five orthogonally located gas holes. Four different hole configurations were studied. The transient heat transfer study employs an IR-camera to determine the local heat transfer coefficient inside each hole. Velocity measurements and numerical flow simulation were used to better understand the measured heat transfer distribution inside the hole. The Nusselt number distribution along the hole surface exhibits significant circumferential non-uniformity associated with impingement and separation, with localized high heat transfer regions caused by flow impingement. The heat transfer coefficient was observed to be a strong function of the Reynolds number, but a weak function of the blowing ratio.

**NOMENCLATURE**

BR	Blowing Ratio ( $\overline{V}_L/V_{\text{crossflow}}$ )
D	Gas hole diameter (mm)
h	Heat transfer coefficient ( $\text{W}/\text{m}^2 \cdot \text{K}$ )
k	Thermal conductivity ( $\text{W}/\text{m} \cdot \text{K}$ )
L	Gas hole length (mm)
Nu	Nusselt number inside gas hole
$\overline{Nu}$	Averaged Nusselt number inside each

hole	
r	Radial distance inside gas hole (mm)
Re	Reynolds number of gas holes
$\overline{Re}$	Averaged Reynolds number of all holes
$Re_L$	Local Re in gas hole (from predictions)
T	Temperature (K)
t	Time (s)
V	Velocity (m/s)
$\overline{V}$	Average velocity (Y-direction) in holes (m/s)
Y	Local coordinate along hole length (mm)

**Subscript**

0	Reference state
$\infty$	Bulk conditions inside gas hole
crossflow	Measured inside the cross flow
L	Locally calculated inside each gas hole
w	At wall

**Greek**

$\alpha$	Thermal diffusivity
----------	---------------------

**INTRODUCTION**

In gas turbines the basic configuration of a row of jets discharging into a crossflow (Figure 1) is encountered in a number of components. The leading edge of an airfoil, for example, has rows of coolant holes fed from a radial-internal passage in the airfoil. The radial feed flow turns at an angle into the coolant holes before discharging orthogonally into the crossflow. Typically the coolant flow is at the compressor-discharge temperature ( $370\text{-}480^\circ\text{C}$ ) while the crossflow is at the combustion-discharge temperature of nearly

1370-1480°C. This leads to large temperature gradients across the coolant holes, and potentially large thermal stresses in regions of high heat transfer coefficients inside the holes. Another example is the fuel-air premixing device where gaseous fuel is injected at almost 90-degrees through distributed holes along fuel-spokes into the crossflow. In this application, the crossflow is at a higher temperature than the gaseous fuel, with the potential for large thermal stresses inside the fuel-delivery holes where the heat transfer coefficient is high.

The above examples motivate the need to examine the heat transfer coefficients inside the gas or coolant holes. This information is useful in assessing the importance of thermal stresses as well as the extent of cooling/heating that is achieved inside the holes. The majority of the published literature is focused on the external surface and the behavior of the jet after it discharges from the hole. The present study is focused on the behavior of the flow and heat transfer coefficient inside the gas/coolant holes.

Since the application of interest focuses primarily on the developing heat transfer in a short hole with a complex entry, the relevant literature is rather limited with the majority of the reported studies devoted to more conventional geometry and entry conditions (see Bejan [1]). The heat transfer behavior in the developing region of a long circular pipe has been extensively studied and entry-region correlations have been reported [2-3]. Sparrow & Cur [4], Han & Park [5] and Raisee & Hejazi [6] each studied the effect of sudden contraction on the developing heat transfer in a downstream duct. Their results indicated that a recirculation bubble formed at the contraction point and local heat transfer coefficient reaches its maximum value where the recirculation bubble reattached on the wall.

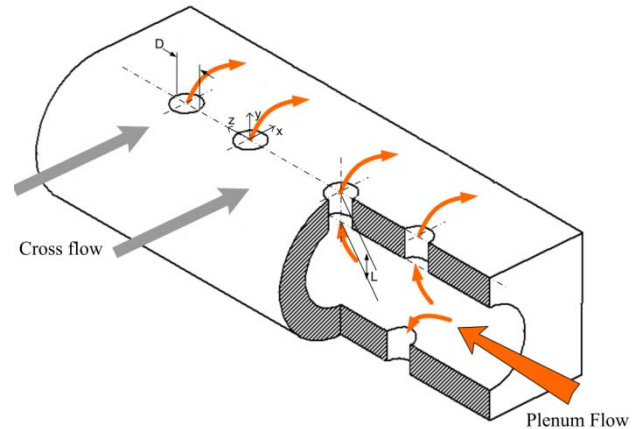


Figure 1. Supply plenum configuration and geometry

Using the naphthalene sublimation method, Cho et al. [7-9] and Goldstein et al. [10] investigated the local heat transfer behavior inside a short hole with different inlet flow configurations. Also, the effect of jet-to-crossflow blowing ratio was investigated. Their results exhibited the existence of a recirculation region inside the hole for Reynolds number less than  $3 \times 10^4$ . Also, the averaged heat transfer coefficient inside the hole was not affected by cross flow for blowing ratio values greater than 0.22.

Peterson & Plesniak [11] and Burd & Simon [12] investigated the effect of plenum geometry and internal flow configuration on film cooling effectiveness outside the coolant hole. Results indicated the significant effect of plenum flow configuration on the flow behavior inside the hole and the heat transfer downstream of the hole. Ramamurthy et al [13] studied the 3-dimensional turbulent flow inside a dividing T-junction numerically and experimentally. His results indicated that the entering flow into the cross branch impinged on one side of the tube inlet and a separation region formed in front of the impingement point. The studies by Kim & Kim [14], Rozati & Tafti [15], Lakehal et al [16], and Lu et al [17] are representative of the literature on leading edge film-cooling. These results indicate the significant effect of the film cooling blowing ratio and hole shapes on the film cooling heat transfer at the blade leading edge.

The objective of the current study is to experimentally examine the behavior and magnitude of the heat transfer coefficient inside gas holes discharging orthogonally into a crossflow as shown in Figure 1 for a range of Reynolds number,

blowing ratio and hole configurations. The configuration has open holes on both sides representing the pressure and suction side surfaces. To better understand the measured distributions, supportive flow measurements and numerical simulations are conducted. This information is expected to provide an improved understanding of the heat transfer behavior and the associated thermal stresses inside the holes.

## EXPERIMENTS

The geometry considered in the present study is shown in Figure 1. The air flowing in the plenum enters the gas holes and discharges into the cross flow. The length (L) and diameter (D) of the holes were identical leading to  $L/D=1$ . The averaged gas hole Reynolds number based on hole diameter ranged from  $0.5 \times 10^5$  to  $2 \times 10^5$ . Blowing ratio, defined as mean hole velocity over cross flow velocity just upstream the holes, was varied from 1.3 to 3.2. The overall size of the test model was  $16.5 \times D$  along the plenum feed-tube,  $6 \times D$  along the cross flow, and  $5 \times D$  along the thickness (normal to the crossflow). It was made out of black Acetal with thermal conductivity of 0.3 W/m-K to satisfy the semi-infinite heat conduction assumption in the body as needed by the transient experimental technique described later. The geometry consisted of four holes on one side and three on the other. All measurements were done for five open holes only, with three open on one side and two on the other. Experiments were performed for four different hole configurations by blocking different holes.

Static pressure data was taken along the feed tube wall before and after each gas hole using an OMEGA HHp 240 pressure module. The pressure tap holes were placed 4mm apart from the hole inlet. The flow velocity inside the gas holes was measured by a Pitot static tube to investigate the flow patterns and to validate the numerical simulation results. The Pitot tube area blockage inside the hole is less than 0.04%, and therefore has negligible blockage effects.

For heat transfer measurement inside the gas hole a transient heat conduction test was performed. The basis of these transient tests is to suddenly expose the test surfaces to heated air and to record the surface temperature with time. Assuming the test surface to be a one-dimensional semi-infinite

body, the corresponding transient heat conduction equation was solved inside the solid body to determine the heat transfer coefficient. The transient temperature distribution is given by [17, 18]:

$$\frac{(T_w - T_0)}{(T_\infty - T_0)} = 1 - \exp\left(\frac{h^2 \alpha t}{k^2}\right) \operatorname{erfc}\left(\frac{h\sqrt{\alpha t}}{k}\right) \quad (1)$$

In this equation  $T_w$  is the wall temperature at each time,  $T_0$  is the wall initial temperature and  $T_\infty$  is the instantaneous bulk flow temperature in the gas hole. In a real experiment, a perfect step change in mainstream flow temperature is impossible. Therefore the time variance in mainstream temperature is taken care by modifying equation (1) using Duhamel's integration [20]. The bulk flow temperature is measured by T-type thermocouples placed along the centerline of the hole. The thermocouple bead and holder size together are less than 3% of the gas hole diameter, and therefore do not influence the flow field in the gas hole. Three thermocouples were installed on the test geometry to ensure temperature uniformity inside the geometry before running the test. Thermocouple data was recorded by a national instrument SCXI-1600 data acquisition module. In order to initiate the transient tests, the plenum flow was heated up to the desired temperature by a 26 KW inline heater and by-passed until the desired temperature was reached. To start the experiments, the bypass valve was flipped diverting the heated flow on to the test surfaces. The test duration was kept to 30 seconds which maintained small thermal penetration depths in the Acetal to satisfy the one-dimensional assumption.

A FLIR SC4000 series IR camera was employed to capture wall temperature inside the holes. The camera is positioned outside the tunnel and views the inside hole surface through a zinc selenide (Zn-Se) window. For each test the camera is positioned so that it views one fourth of the gas hole inner surface area. Therefore, four test runs were required to cover the entire hole surface area. Camera calibration was performed in-situ (using surface-mounted thermocouples inside the holes) before running the tests. A calibration curve was generated by FLIR EXAMIN-IR MAX software to

relate the surface temperature to the IR emission intensity.

The standard uncertainty based on 95% confidence level was calculated by a combination of the uncertainties of all inputs based on the method described by Kline & McClintock [19]. The standard uncertainty in temperature reading was  $\pm 0.5^\circ\text{C}$  and for time was  $\pm 0.1$  s. The maximum uncertainty in heat transfer coefficient with IR thermography method was calculated to be  $10.0 \pm 2\%$ . The repeatability error was about 5% between repeated tests. The standard uncertainty in pressure reading was  $\pm 0.01$  kPa.

### NUMERICAL SIMULATION

For improved understanding of the flow field inside the gas holes, numerical simulation using the commercial code FLUENT was employed. The incompressible flow equations were solved using the high Reynolds number realizable  $k-\epsilon$  turbulence model. Non-equilibrium wall functions were used to model the wall effects on the turbulent flow. The realizable  $k-\epsilon$  model provides superior performance for flows involving boundary layers under strong adverse pressure gradients and separation. Moreover, due to the capability to partly account for the effects of pressure gradients, the non-equilibrium wall functions are recommended for use in complex flows involving separation and reattachment [21-23].

Hexahedral grid cells were generated using ANSYS-ICEM software inside the simulation domain. The wall  $Y^+$  value was kept in the range of 30 to 100 to satisfy the requirements for the turbulence model. Figure 2-a shows the numerical grid distribution at the gas hole exit. In Figures 2-b&c the grid pattern inside the gas hole and on the plenum wall is presented. To investigate the effect of grid density on the flow parameters, flow simulation inside one gas hole was performed for different grid sizes ranging from  $0.4 \times 10^6$  to  $2 \times 10^6$  cells. Variation of wall shear stress inside the hole for different grid densities is presented in Figure 3 for  $\overline{Re} = 1.7 \times 10^5$  and  $BR = 2.65$ . Results indicate that beyond 1.0 million cells no significant variation in

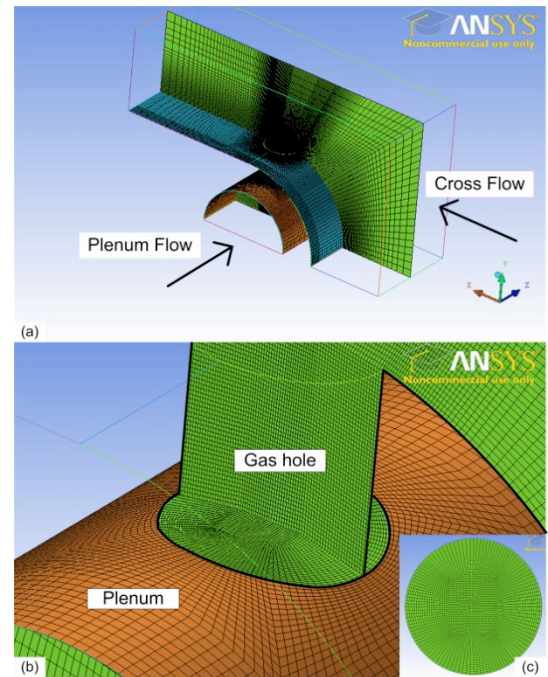


Figure 2. Numerical grid distribution inside and around one gas hole

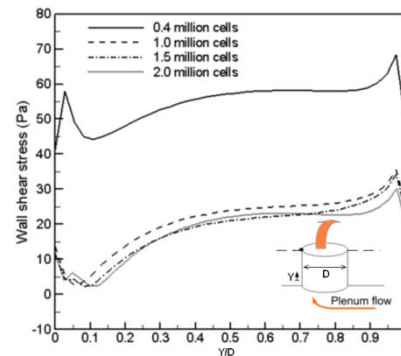


Figure 3. Variation of wall shear stress for different grid densities ( $\overline{Re} = 1.7 \times 10^5$ )

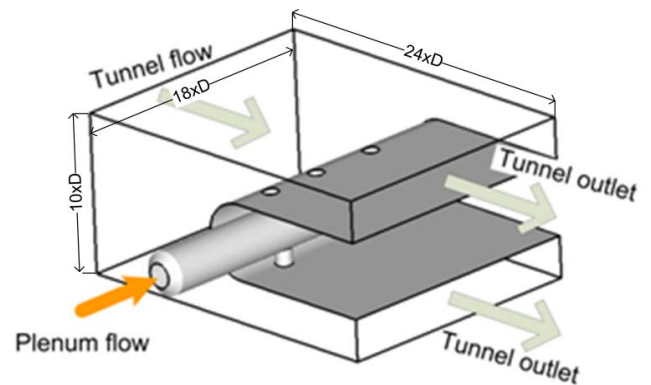


Figure 4. Numerical simulation domain for complete test geometry

the shear stress is observed. These grid independence results were also applicable in similar studies at lower Reynolds numbers. Based on the conclusion that nearly 1 million cells are needed for one single hole, the grid size was appropriately

extrapolated for the complete 5 hole geometry. The numerical domain and boundary conditions for whole test section is shown in Figure 4. Nearly 6 million cells were used for these calculations.

## RESULTS AND DISCUSSION

Results will be presented initially for the baseline configuration (labeled configuration A), for a range of Reynolds numbers based on an estimated equi-distribution of flow through each hole ( $\overline{Re}$ ) and for different blowing ratios (BR, defined as the ratio of the gas-hole velocity to the cross-flow velocity). Where noted in the text, a local hole-Reynolds number  $Re_L$  based on the local predicted mass flow rate through each hole is also utilized.

**Pressure Data:** The measured values of the feed-tube surface pressures are shown in Figure 5. As shown, the pressure at the fore-side of each hole inlet was lower than that of the aft-side. This trend was consistent for all 5 holes experimentally. Low pressure on the fore-side of the hole indicates the flow acceleration while turning into the hole. At the aft-side of the hole the turning flow impinges on the wall leading to higher pressure values (Ramamurthy et al [13]).

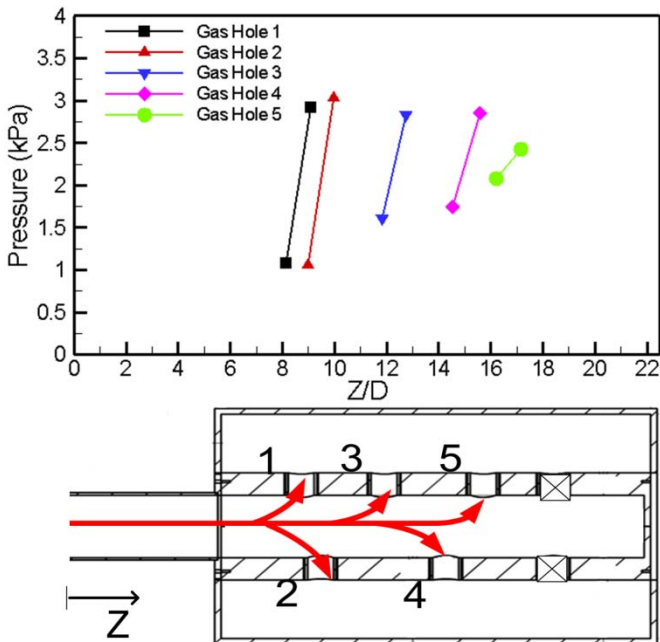


Figure 5. Experimental pressure inside the plenum on either side of the gas holes, ( $\overline{Re} = 1.7 \times 10^5$ ). For each hole, the lower pressure value represents the fore side and the higher pressure value represents the aft-side of the hole inlet.

**In Hole Velocity Field:** Velocity field inside holes was obtained with a pitot probe oriented along the gas hole direction. Figures 6a & 6b show the normalized velocity distribution inside holes 1 to 5 for different Reynolds numbers along two perpendicular (to the flow) lines at  $Y/D=0.5$ . The velocity values were normalized by the averaged velocity in the holes (estimated using the feed tube mass flow rate). The RANS prediction results for two Reynolds numbers are shown by the dashed lines.

It should be noted that since the pitot-static probe is oriented toward the feed hole, it can only measure the positive Y-direction velocity oriented from the feed tube toward the crossflow. Negative velocities cannot be measured and are arbitrarily set to zero here. Therefore, inside each gas hole (1 to 5) at some points for  $2r/D$  greater than 0.5 the measured Y-velocity was set to zero implying a recirculation region. Velocity distribution inside holes 1 to 5 along line “I”, indicates existence of a separation region inside holes, which was formed at the hole inlet (as also observed by Cho et al [7-9] and Ramamurthy et al [13]) on the forward side of the hole. The numerical results at the two Reynolds number shown are in good agreement with the data and appear to indicate a Reynolds number effect on the size and strength of the separated zone. In general, the recirculation region appears to decrease for holes that are progressively further from the inlet. The velocity distribution in the fifth hole is distinctly different than those in the earlier holes. This hole sees a more symmetric entry flow (since the downstream end of the feed tube is blocked and flow enters the last hole from both the fore and the aft side of the hole). Associated with the more symmetric entry, the velocity profiles show their peak velocities close to the hole centerline rather than on the leeward (impingement) side of the hole. Along the centerline “C”, the velocity profiles are generally symmetric for all holes.

Figure 7 shows predicted normalized Y-velocity contour maps and stream traces inside each hole along the I-plane and the C-plane. To preserve clarity in the contours, all zero and negative velocity are color coded by a single blue color. In holes 1 to 4, the separation region on the forward side of the hole is clearly evident along I-plane, and appears to extend the entire length of the hole.

Along C-plane, the velocity distributions appear quite symmetric as seen earlier in the line plots and the pitot-static measurements.

Holes 1 and 2 see the highest turning velocity, and therefore the larger separation zone. Stream traces indicate that for these two holes, the plenum flow was divided at the hole inlet, and the entering flow into the hole 1 and 2 strongly impinged the aft-side of the hole with a significant separation on the fore-side of the hole. In hole 3, as seen in Figure 7, a weak flow leaks into the hole from the aft-side. This indicates that flow impingement on the aft-wall is not as strong as in holes 1 and 2. In hole 4, a weak flow turns into the hole from the aft-side and generates a very small separation bubble on this side of the hole. This small separation region alters the velocity profile and pushes the peak of the velocity profile to the hole center. In this hole, flow does not directly impinge on the aft-side of the hole, and one would expect lower and more distributed heat transfer coefficients.

In the 5<sup>th</sup> hole, as noted earlier, the entry flow is more symmetric, and the flow turning into the hole from the aft-side is strong enough to form a significant separation bubble on that side of the hole. Because of the recirculation, maximum velocity value was shifted to the hole center and velocity profile looks symmetric. As shown in Figure 7-a, velocity profile in gas holes changes from a non-symmetric profile in hole 1 to near-symmetrical in hole 5. Also the fore-vortex size at the hole inlet, shown in Figure 7-a, decreases from hole 1 to hole 5. In Figure 7-a the flow impingement region on aft side of the hole is indicated by two red horizontal lines. This impingement region is associated with the largest velocity gradients and heat transfer coefficients as discussed in the next section.

**Heat Transfer:** Heat transfer coefficient measured was non-dimensionalized as a Nusselt number using the hole diameter as the length scale. Figure 8 shows the normalized Nusselt number contour map inside holes 1 to 5 for different  $Re$ . Nusselt number values were normalized by the fully developed turbulent pipe flow Nusselt number [1] at the corresponding Reynolds number. Circumferential non-uniformity in  $Nu/Nu_0$  distribution is seen in Figure 8 inside the gas holes

1-4 due to the non-uniform velocity profiles in the holes. In these plots, the gas holes are unwrapped around the impingement line of 0-degrees.

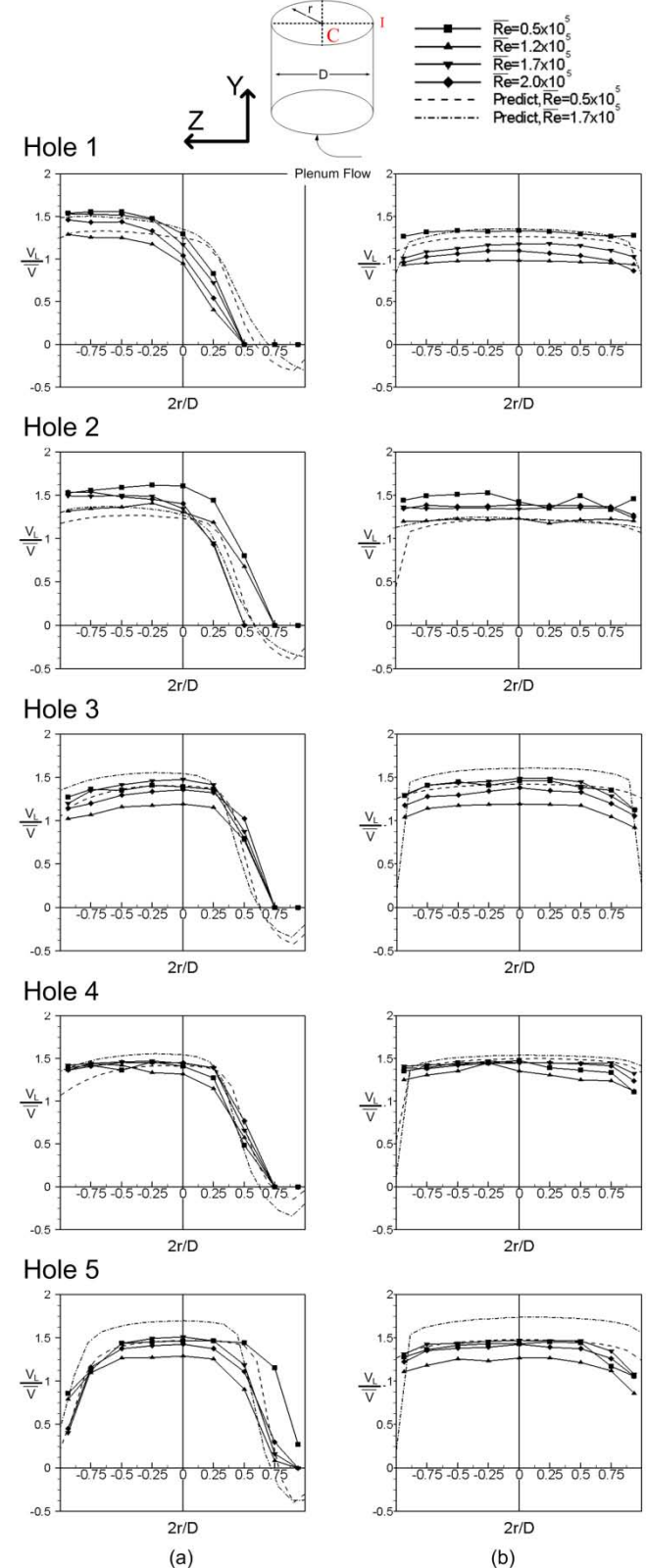


Figure 6. Normalized velocity distribution inside the holes 1 to 5 for the baseline configuration at different Reynolds numbers a) along line "I", b) along line "C"

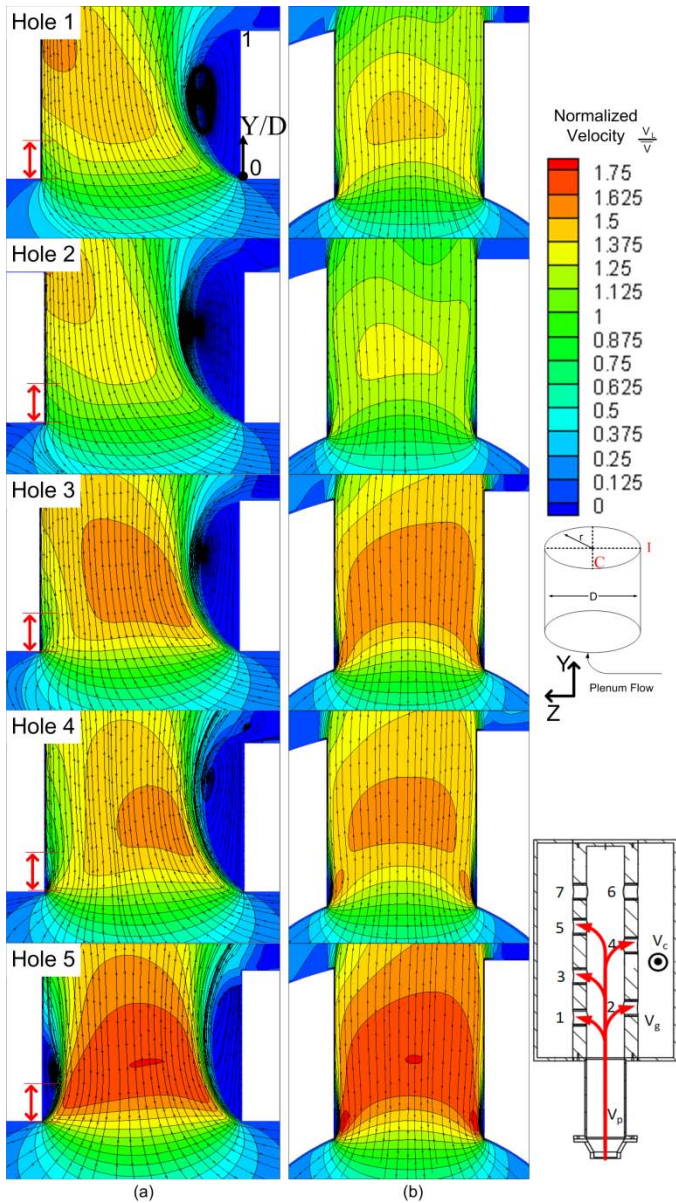


Figure 7. Y-velocity contours and stream lines in holes 1 to 5 a) Along I-plane (Flow impingement region placed between red lines on left) b) along C-plane ( $\overline{Re} = 1.7 \times 10^5$ )

Nusselt numbers are typically high in regions where the flow impinges (vicinity of 0-degrees) and low in the separated regions (near 180 degrees) inside the hole. As indicated, for all holes the high  $Nu/Nu_0$  value region was more spread out and distributed for  $\overline{Re} = 0.5 \times 10^5$  than  $\overline{Re} = 2.0 \times 10^5$ . By increasing the  $\overline{Re}$  number, the recirculation region size increases and expands the low  $Nu/Nu_0$  region inside the holes leading to greater circumferential non-uniformity.

For holes 1 to 4, the heat transfer peak values typically exists in the region  $-45^\circ < \theta < +45^\circ$  and  $0 < Y/D < 0.25$ . In holes 1 and 2 the heat transfer

peak magnitudes are the highest due to the strong flow impingement as discussed earlier in relation to Figure 7. In hole 3, the peak values begin to diminish but only slightly. For the 4<sup>th</sup> hole, the flow pattern was different due to small vortex on the aft-side of the hole inlet (Figure 7), and the peak  $Nu/Nu_0$  values are lower and the distributions are more uniform. In hole 5, velocity profile was near symmetrical (Figures 6 and 7), there is no flow impingement and local  $Nu/Nu_0$  distributions are approximately uniform in the gas hole.

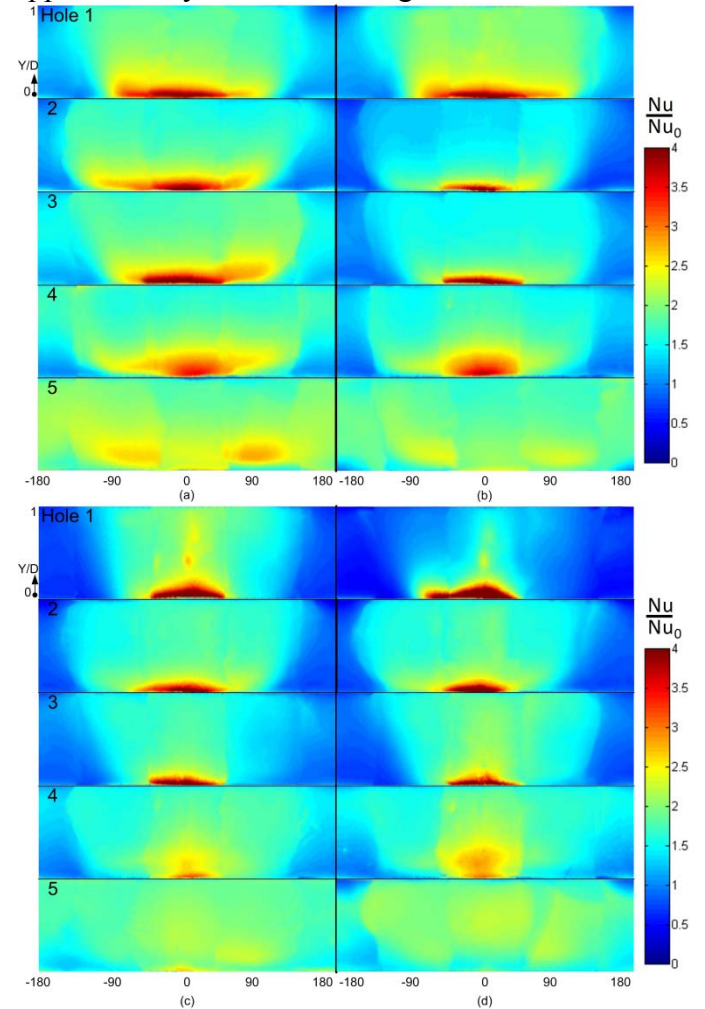


Figure 8. Normalized Nusselt number in hole contour maps for configuration A, a)  $\overline{Re} = 0.5 \times 10^5$ , b)  $\overline{Re} = 1.2 \times 10^5$  c)  $\overline{Re} = 1.7 \times 10^5$ , d)  $\overline{Re} = 2.0 \times 10^5$ . For clarity contour levels have been capped at a maximum of 4, and values greater than 4 all appear at color levels corresponding to the maximum.

The high  $Nu/Nu_0$  region at the inlet of gas holes on the aft-side plays a significant role on the non-uniformity in the circumferential  $Nu/Nu_0$  distribution inside the holes. Figure 9 shows the variation of maximum Nu ratio on the aft-side of the hole versus local Reynolds number while Figure 10 shows the circumferential distribution of Nusselt

number ratio at the hole inlet. The local Reynolds number here was calculated based on predicted mass flow rate in each gas hole.

In holes 1 to 3, Figure 9 shows that high values of the peak Nu are observed due to flow impingement on the hole aft-wall. Figure 9 indicates that the heat transfer value at the impingement region of holes 1 to 3 was similar at the lower Reynolds numbers ( $Nu/Nu_0 \sim 5$ ). For holes 1 and 2, the  $Nu/Nu_0$  ratio increases sharply beyond a critical  $Re_L$  value, and indicate that for the first two holes, impingement effects are dominant beyond a certain  $Re_L$  and do not follow the  $Re_L^{0.8}$  correlation for a turbulent pipe flow. However for holes 3 to 5, the normalized peak Nusselt number value remains relatively constant versus  $Re_L$  indicating that for these holes that are farther from the feed inlet the turbulent pipe scaling with  $Re_L$  is applicable. Due to the recirculation regions and its hole-to-hole variation, the  $Re_L$  increases from hole 1 to 5.

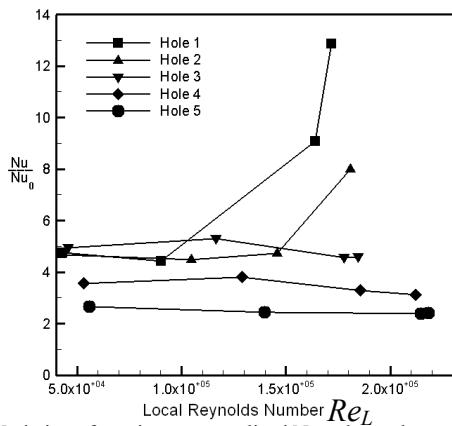


Figure 9. Variation of maximum normalized Nusselt number on the aft-side vs local Reynolds number

Measured and predicted circumferential variation of normalized Nusselt number at  $Y/D=0.05$  (short distance from the hole inlet), as presented in Figure 10, indicate large circumferential non-uniformity in the Nu distribution at the inlet of hole 1. Peak  $Nu/Nu_0$  values are as high as 8 associated with the strong impingement effect for this hole. By moving down the feed tube from hole 1 to hole 5, the differences in the Nu distribution at the hole inlet reduces and a uniform near-flat distribution is observed for hole 5 where, as seen in Figure 7, no flow impingement is seen to occur near the hole entry. In general, the predictions of the Nusselt number shown indicate good agreement with the measured data.

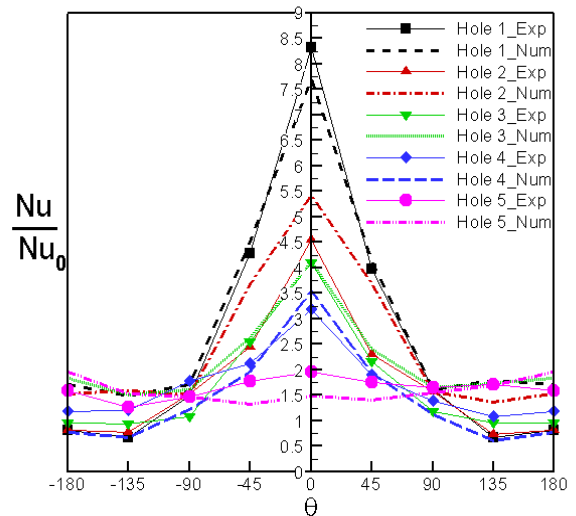


Figure 10. Circumferential Variation of  $Nu/Nu_0$  at the inlet of gas holes 1 to 5 ( $Re = 1.7 \times 10^5$ )

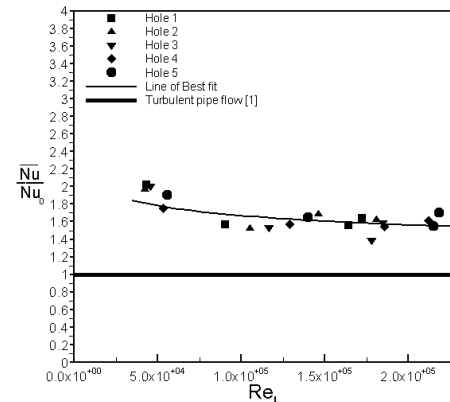


Figure 11. Variation of normalized Nusselt number vs local Reynolds number

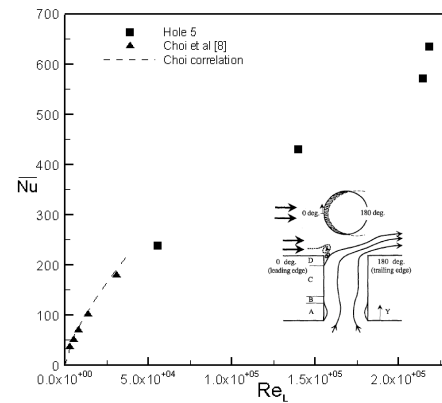


Figure 12. Averaged Nusselt number inside hole 5 and a short hole with axisymmetrical entrance flow versus local Reynolds number

Variation of the hole-averaged Nusselt number ratio versus  $Re_L$  is presented in Figure 11. As shown in the figure, all the measured data are in a narrow band and scale well with the  $Re_L$ . At the higher Reynolds number the Re-scaling appears to be consistent with the pipe flow scaling. At the

lower  $Re_L$  ( $<1.5 \times 10^5$ ), the Re-dependence shows a greater than the 0.8 pipe flow exponent. In hole 5, because of the near-symmetrical velocity profile inside the hole, averaged Nusselt numbers inside the 5<sup>th</sup> hole was combined with that of measured data for symmetric flow contraction into a short hole (Cho et al [8]). The data in [8] is at  $Re_L$  values below  $5 \times 10^5$  while the present data for hole 5 is for larger  $Re_L$  values. Figure 12 also shows the correlation curve reported by Cho et. al. in the relevant Re-range. In general, the data in Figure 12 indicates that the Nusselt number ratio shows a consistent Re-correlation over an extended Re range for a short hole with axi-symmetrical entry flow.

The effect of blowing ratio on the average heat transfer was investigated for BR ranging from 1.3 to 3.2. Figure 13 shows the variation of averaged Nusselt number in holes 1 and 5 vs. blowing ratio. Results indicate that for blowing ratio greater than 1.3 averaged Nusselt number variation with BR was negligible (Cho et al [8]).

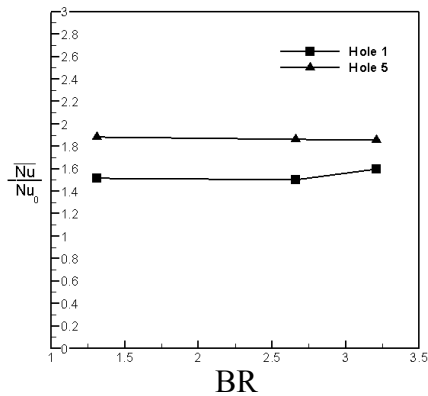


Figure 13. Variation of Normalized Nusselt number in holes 1 and 5 vs blowing ratio ( $\overline{Re} = 1.7 \times 10^5$ )

**Hole Configurations:** In addition to basic configuration (labeled A) for which results have been presented above, three other configurations shown in Figure 14 were investigated at  $\overline{Re} = 1.7 \times 10^5$ . These configurations are shown with seven holes of which only five are open. In configuration A, the last two holes (6 and 7) are closed. In the other three configurations studied, labeled B, C and D, different combinations of five holes are open as shown in Figure 14.

Figure 15 shows the  $Nu/Nu_0$  contour maps in each hole for different configurations. In all cases variation in  $Nu/Nu_0$  contour maps from first to last

hole was similar to basic configuration (A). In all arrangements, the last hole had a more uniform  $Nu$  distribution than other holes. In configuration (D), local  $Nu$  distributions in holes 6 and 7 were identical because these holes are exactly at the same distance from the plenum end, and in front of each other.

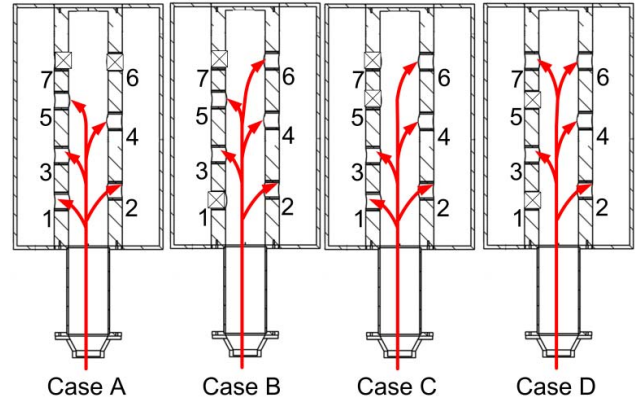


Figure 14. Hole-arrangement in different configurations

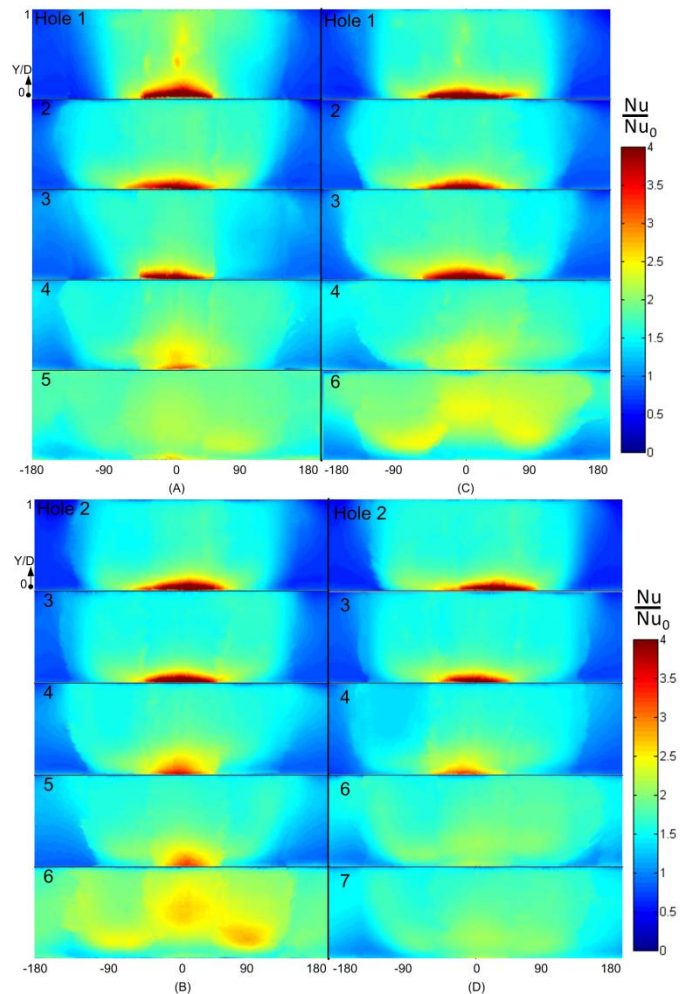


Figure 15.  $Nu/Nu_0$  contour maps inside each hole for configurations A, B, C and D. For clarity contour levels have been capped at a maximum of 4, and values greater than 4 all appear at color levels corresponding to the maximum. ( $\overline{Re} = 1.7 \times 10^5$ )

Averaged normalized Nusselt number for all holes at  $\overline{Re}=1.7 \times 10^5$  is shown in Figure 16. For all configurations, the averaged values follow an increasing trend from the first hole to the last one. This rising trend of the averaged Nusselt number is linked to the size of the recirculation region and the mass flow rate through each gas hole. In general, the  $\overline{Nu}$  values for the first four holes in configurations A and C and the first three holes in configurations B and D were within the uncertainty range. The averaged normalized Nusselt number values in two last holes of configuration (D) were the same due to identical hole positions in the feed tube.

In configuration (D) the averaged heat transfer value from hole 1 to 5 shows lower values than other configurations. Therefore, this configuration of holes has the lowest Nusselt number and lower non-uniformities (see Figure 16) in the circumferential direction.

**SUMMARY:**

Heat transfer and fluid flow inside gas holes discharging orthogonally into a crossflow was studied experimentally and numerically. The effect of Reynolds number, blowing ratio and hole configuration on the heat transfer inside the gas holes were investigated. Pressure and velocity measurements inside each hole were performed for improved understanding of the in-hole heat transfer contour maps. The following major conclusions were made from this study:

- 1- The flow entering the first three holes of all configurations impinges along the aft-side of the holes. The resulting heat transfer coefficient and Nu value is very high at the impingement point with peak  $Nu/Nu_0$  generally in the range of 4-8.
- 2- For gas holes 1-3, the flow turning and impingement on the aft-side is associated with flow separation on the leading side of the hole where  $Nu/Nu_0$  values are low (<1).
- 3- For gas holes closest to the end of the feed tube (holes 4 and 5 for configuration (A)), the flow into the gas hole is more symmetric leading to more uniform Nu distributions.
- 4- The local heat transfer distribution inside gas holes changes from a highly non-uniform

circumferential distribution inside hole 1 to a nearly uniform distribution in hole 5.

- 5- Among all four different hole configurations, arrangement (D) exhibits lower averaged heat transfer values from 1<sup>st</sup> to 5<sup>th</sup> hole.
- 6- The blowing ratio does not affect the heat transfer coefficient inside the holes.

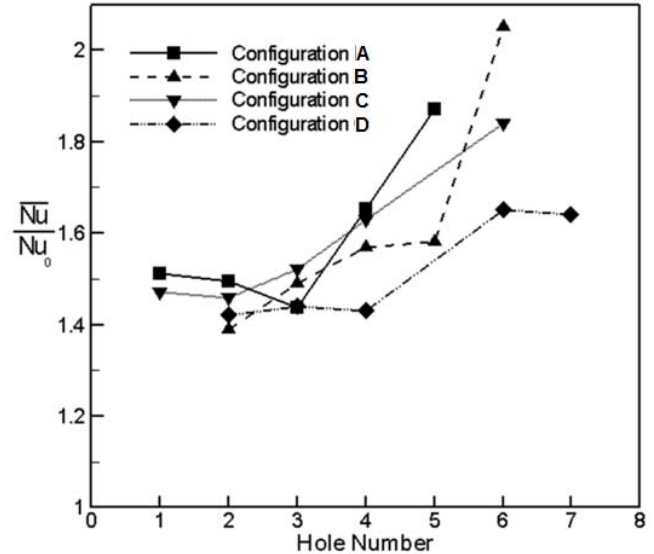


Figure 16. Averaged normalized Nusselt number in holes for different configurations ( $\overline{Re}=1.7 \times 10^5$ )

**ACKNOWLEDGEMENTS:**

This work was supported by a grant from Siemens Energy. This support is gratefully acknowledged. We appreciate the support and guidance received from our technical monitor Reinhard Schilp and several other Siemens personnel including Chander Prakash and Mike Crawford.

The content of this paper is copyrighted by Siemens Energy, Inc. and is licensed to ASME for publication and distribution only. Any enquiries regarding permission to use the content of this paper, in whole or in part, for any purpose must be addressed to Siemens Energy, Inc. directly.

**REFERENCES:**

- 1- Bejan, A., 2004, "Convection heat transfer" , *John Wiley & Sons*
- 2- Al-Arabi, M., 1982, "Turbulent heat transfer in the entrance region of a tube" *Heat transfer Engineering*, Vol 3, pp. 76-83
- 3- Ghajar, A. J., Tam, L. M., 1994, "Heat transfer measurement and correlations in the transient region for a circular tube with three different inlet configurations" *Experimental Thermal and Fluid Science*, vol 8, 1, pp. 79-90,

- 4- Sparrow, E. M., Cur, N., 1982, "Turbulent heat transfer in a symmetrically or asymmetrically heated flat rectangular duct with flow separation at inlet" *Journal of heat transfer*, vol 104, 1, pp. 82-89
- 5- Han, J. C., Park, J. S., 1988, "Developing heat transfer in rectangular channels with rib turbulators", *International journal of heat and mass transfer*, vol 31, 1, pp. 183-195
- 6- Raisee, M., Hejazi S. M., 2007, "Application of linear and non-linear low-Re k- $\epsilon$  models in two dimensional predictions of convective heat transfer in passages with sudden contractions", *International journal of heat and fluid flow*, vol 28, 3, pp. 429-440
- 7- Cho, H. H., Jabbari, M. Y., Goldstein, R. J., 1997, "Experimental mass(heat) transfer in and near a circular hole in a flat plate" *International journal of heat and mass transfer*, vol 40,10, pp. 2431-2443
- 8- Cho, H. H., Goldstein, R. J., 1995, "Heat (mass) transfer and film cooling effectiveness with injection through discrete holes: part I-Within holes and the back surface" *Journal of turbomachinery*, vol 117, 3, pp. 440-450
- 9- Cho, H. H., Kang, S. G., Rhee, D. H., 2001, "Heat/mass transfer measurement within a film cooling hole of square and rectangular cross section" *Journal of turbomachinery*, vol 123, 4, pp. 806-814
- 10- Goldstein, R. J., Cho, H. H., Jabbari, M. Y., 1997, "Effect of plenum crossflow on heat (mass) transfer near and within the entrance of film cooling holes" *Journal of turbomachinery*, vol 119, 4, pp. 761-769
- 11- Peterson, S. D., Plesniak, M. W., 2002, "Short hole jet in crossflow velocity field and its relationship to film cooling performance" *Experiments in fluids*, vol 33, 6, pp. 889-898
- 12- Burd, S. W., Simon, T. W., 1997, "The Influence of Coolant Supply Geometry on Film Coolant Exit Flow and Surface Adiabatic Effectiveness" *ASME Paper No. 97-GT-25*.
- 13- Ramamurthy, A. S., Qu, J., Vo, D., Zhai, C., 2006, "3-D simulation of dividing flows in 90 deg rectangular closed conduits" *Journal of fluids engineering*, vol 128, 5, pp. 1126-1129
- 14- Kim, Y. J., Kim, S.M., 2004, "Influence of shaped injection holes on turbine blade leading edge film cooling" *International journal of heat and mass transfer*, vol 47,2,pp. 245-256
- 15- Rozati, A., Tafti, D.K., 2008, "Large-eddy simulations of leading edge film cooling: Analysis of flow structures, effectiveness, and heat transfer coefficient" *International journal of heat and fluid flow*, vol 29,1,pp. 1-17
- 16- Lakehal, D., Theodoridis, G.S., Rodi, W., pp. 2001, "Three-dimensional flow and heat transfer calculations of film cooling at the leading edge of a symmetrical turbine blade model" *International journal of heat and fluid flow*, vol 22, 2, pp. 113-122
- 17- Lu, Y., Allison, D., Ekkad, S.V., 2007, "Turbine blade showerhead film cooling: Influence of hole angle and shaping" *International journal of heat and fluid flow*, vol 28, 5, pp. 922-931
- 18- Acharya. S., Kramer, G., Moreaux, L., Nakamata, C., 2010, "Squealer tip heat transfer with film cooling: *Proceeding of ASME Turbo Expo 2010*, June 14-18, Glasgow, UK
- 19- Kline, S. J., McClintock, F. A., 1953, "Describing experimental uncertainties in single sample experiments", *Mechanical Engineering*, vol 75, 1, pp. 3-8
- 20- Ekkad, S.V, Han, J.C., 2000,"A transient liquid crystal thermography technique for gas turbine heat transfer measurements" *Measuring Science Technology*, vol 11, pp. 957-968
- 21- Fluent Inc., "FLUENT 6.3 user guide", Fluent Inc., September 2006
- 22- Kim, J. Y., Ghajar, A. J., Tang, C., and Foutch, G. L., 2005, "Comparison of near-wall treatment methods for high Reynolds number backward-facing step flow", *Int. J. Comp. Fluid Dynamics*, vol. 19-7, pp. 493-500
- 23- Acharya, S., Hoda, A., Tyagi, M., "Flow and Heat Transfer Predictions of Film Cooling", in *Heat Transfer in Gas Turbine Systems*, Annals of the New York Academy of Sciences, Vol. 934, 2001, pp. 110-125 (Editors: R. J. Goldstein and T. Simon)